Journal of Applied Physics

RESEARCH ARTICLE | NOVEMBER 01 2021

Epitaxial lateral overgrowth of *r*-plane α-Ga_2O_3 with stripe masks along $\langle \bar{1}2\bar{1} \rangle$

Special Collection: Wide Bandgap Semiconductor Materials and Devices

Yuichi Oshima ; Shingo Yagyu; Takashi Shinohe

J. Appl. Phys. 130, 175304 (2021)
https://doi.org/10.1063/5.0068097

Journal of Applied Physics ARTICLE scitation.org/journal/jap

Epitaxial lateral overgrowth of *r*-plane α-Ga_2O_3 with stripe masks along $\langle \bar{1}2\bar{1}0 \rangle$

Cite as: J. Appl. Phys. **130**, 175304 (2021); doi: 10.1063/5.0068097
Submitted: 23 August 2021 · Accepted: 12 October 2021 ·
Published Online: 1 November 2021

Yuichi Oshima,[1,a)] Shingo Yagyu,[2] and Takashi Shinohe[2]

AFFILIATIONS

[1]Optical Single Crystals Group, National Institute for Materials Science, 1-1 Namiki, 305-0044 Tsukuba, Japan
[2]FLOSFIA, Inc., Kyodai-Katsura Venture Plaza, 615-8245 Kyoto, Japan

Note: This paper is part of the Special Topic on: Wide Bandgap Semiconductor Materials and Devices.
[a)]**Author to whom correspondence should be addressed:** OSHIMA.Yuichi@nims.go.jp

ABSTRACT

We demonstrated the epitaxial lateral overgrowth (ELO) of ($\bar{1}012$) (*r*-plane) α-Ga_2O_3 using a striped mask pattern along $\langle \bar{1}2\bar{1}0 \rangle$. α-$Ga_2O_3$ stripes with an asymmetric cross-sectional shape were formed selectively on the windows at the initial growth stage. They grew vertically and laterally to coalesce with each other, and a compact film was obtained. The film surface exhibited wave-like morphology with macro-scale inclined terraces and steps because of the asymmetric cross-sectional stripe shape. The macrosteps moved laterally like traveling waves as the growth proceeded. Transmission electron microscopy revealed that a domain on a window grew toward the inclined *c*-axis direction to cover the adjacent domain after the coalescence. As a result, the dislocations, which propagated into the α-Ga_2O_3 stripe from the seed layer through the window, bent toward the *c* axis and concentrated in a narrow area. This concentration should enhance the pair annihilation. Therefore, the dislocation density was markedly reduced on the top surface including the areas above the windows and coalesced boundaries in contrast to the cases of conventional *c*-, *a*-, and *m*-plane ELO.

I. INTRODUCTION

Corundum-structured α-Ga_2O_3 is one of the metastable phases of Ga_2O_3. This material is an ultra-wide bandgap semiconductor with a bandgap energy of approximately 5.3 eV[1] and so is promising for applications such as power devices and ultraviolet (UV) photodetectors. Indeed, Schottky barrier diodes (SBDs) with very low on-resistance and an excellent ideality factor have been demonstrated in spite of the high dislocation density.[2,3] High-response UV detectors have also been demonstrated.[4,5] In addition, α-$(Al_xGa_{1-x})_2O_3$ solid solutions can be grown without limiting aluminum content *x*,[6] in contrast to β-$(Al_xGa_{1-x})_2O_3$, where *x* is limited to being below ~0.7 for bulk films ($t > 50$ nm) although higher *x* is possible for very thin films ($t < 10$ nm).[7] Therefore, band engineering using α-$(Al_xGa_{1-x})_2O_3$ is possible over a wide range (5.3–8.6 eV) with higher freedom of the film thickness. It is also possible to make a hetero pn junction with corundum-structured p-type oxides such as α-Ir_2O_3, which has a lattice constant close to that of α-Ga_2O_3 ($\Delta a/a \sim 0.1\%$).[8–11] Normally off α-Ga_2O_3-based metal–oxide–semiconductor field-effect transistors (MOSFETs) with a p-type well have been demonstrated,[12] and a high channel mobility of 72 $cm^2\,V^{-1}\,s^{-1}$, which is greater than that of a typical commercially available SiC-based MOSFET, has been reported.[13]

A drawback of α-Ga_2O_3 is the absence of homoepitaxial bulk substrates because this material is metastable under ambient pressure,[14] and so melt-grown bulk α-Ga_2O_3 single crystals are not available, unlike β-Ga_2O_3.[15–18] Accordingly, α-Ga_2O_3 films need to be grown heteroepitaxially. Sapphire substrates are mainly used for the growth because sapphire also has a corundum structure, and large-diameter substrates are available at a reasonable price. Mist chemical vapor deposition, halide vapor phase epitaxy (HVPE), and molecular beam epitaxy have been mainly reported as the growth methods.[1,19–22] However, the dislocation density in a heteroepitaxial α-Ga_2O_3 layer is as high as 1×10^{10} cm^{-2} because of the large lattice mismatch ($\Delta a/a = 4.5\%$, $\Delta c/c = 3.3\%$), if no measure is taken.[23] Such a high density of dislocations can deteriorate the electrical properties and device performance. For example, a relatively large leakage current was reported for α-Ga_2O_3-based SBDs.[2] This result indicates that dislocations could be a current leakage path. In addition, a large drop in the electron mobility has been reported

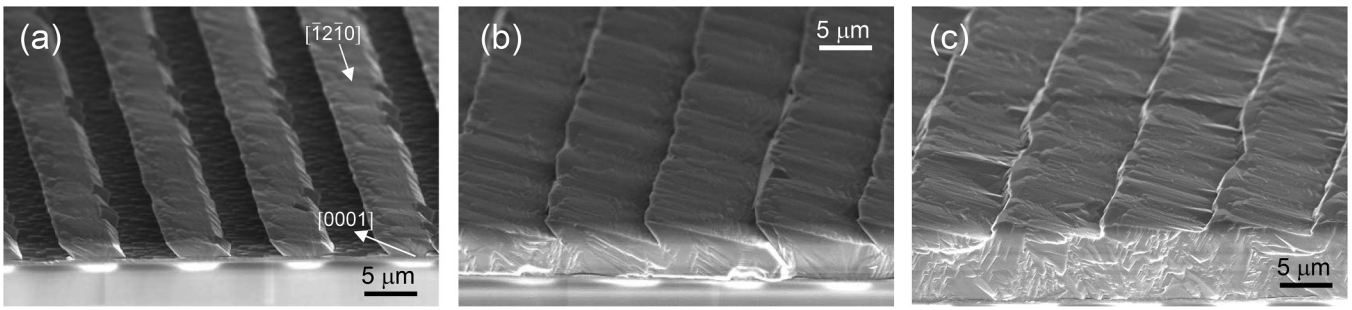

FIG. 1. Bird's-eye view SEM images of *r*-plane α-Ga_2O_3 grown on the striped mask. (a) Formation of isolated α-Ga_2O_3 stripes, (b) just after the coalescence, and (c) thick film growth after the coalescence.

for n-type α-Ga_2O_3 in low concentration regions probably because of the scattering by dislocations.[24] Such mobility drop would be a barrier to achieve high breakdown voltage and low on-resistance at the same time. Furthermore, minority carrier lifetime in a pn junction is likely to be limited because of the dislocations. This limitation could be an obstacle upon optimizing the switching speed and on-resistance. Therefore, the dislocation density needs to be reduced. To decrease the dislocation density, epitaxial lateral overgrowth (ELO) has been investigated, and reported for the growth of *c*-, *a*-, and *m*-plane α-Ga_2O_3 epilayers.[23–29] The ELO technique dramatically decreases the dislocation density in the laterally grown area on the mask, and a very low density of less than $5 \times 10^6\,cm^{-2}$ has been reported.[23] However, the dislocation density above the window remains very high when the α-Ga_2O_3 stripe/island formed on the window has a flat top because the dislocations in the seed layer go up straight to the top surface.[23,28,29] It is possible to bend the dislocations to prevent them from reaching the top surface and suppress the formation of the defective areas by the facet-initiated ELO (FIELO) technique, which was originally developed to improve the crystal quality of heteroepitaxial GaN layers.[30] In the FIELO process, the growth conditions are chosen so that the top part of a stripe/island consists of inclined facets. Then, the dislocations bend to be perpendicular to the facets to minimize the elastic energy along the dislocation line. So far, for α-Ga_2O_3, the FIELO technique has been applied only to the *c*-plane,[23] and the process is successful as long as the stripes/islands are isolated from each other. However, a highly disordered morphology develops after the coalescence leaving deep pits, which are not easily removed by polishing, in contrast to the case of GaN where a smooth surface can be easily recovered. As an alternative approach, the double-ELO technique has been demonstrated.[31] In this technique, the second mask is designed so that the window areas are located only on the

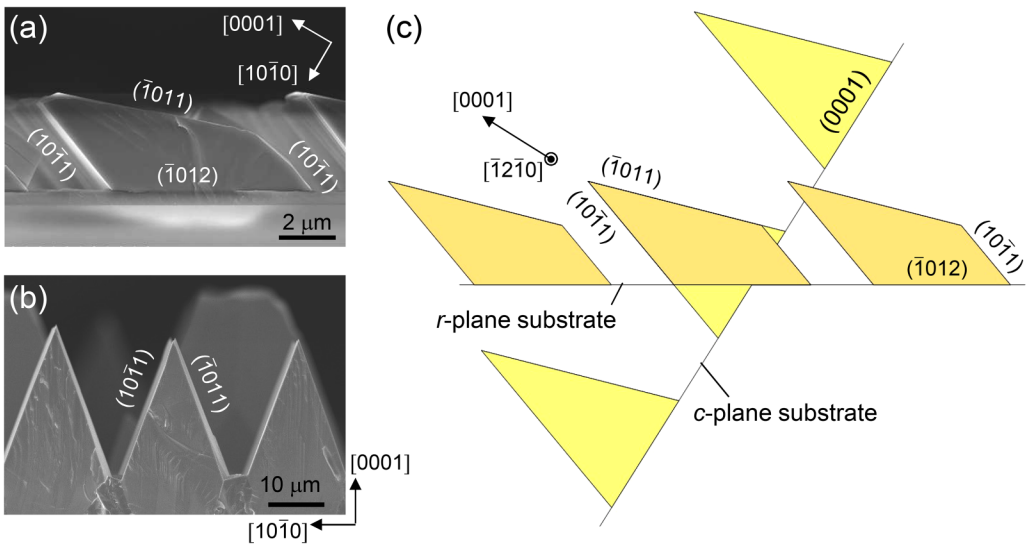

FIG. 2. (a) and (b) Cross-sectional SEM images of the α-Ga_2O_3 stripes along [$\bar{1}2\bar{1}0$] grown on *r*- and *c*-plane sapphire, respectively. (c) Schematic comparing the facet structures.

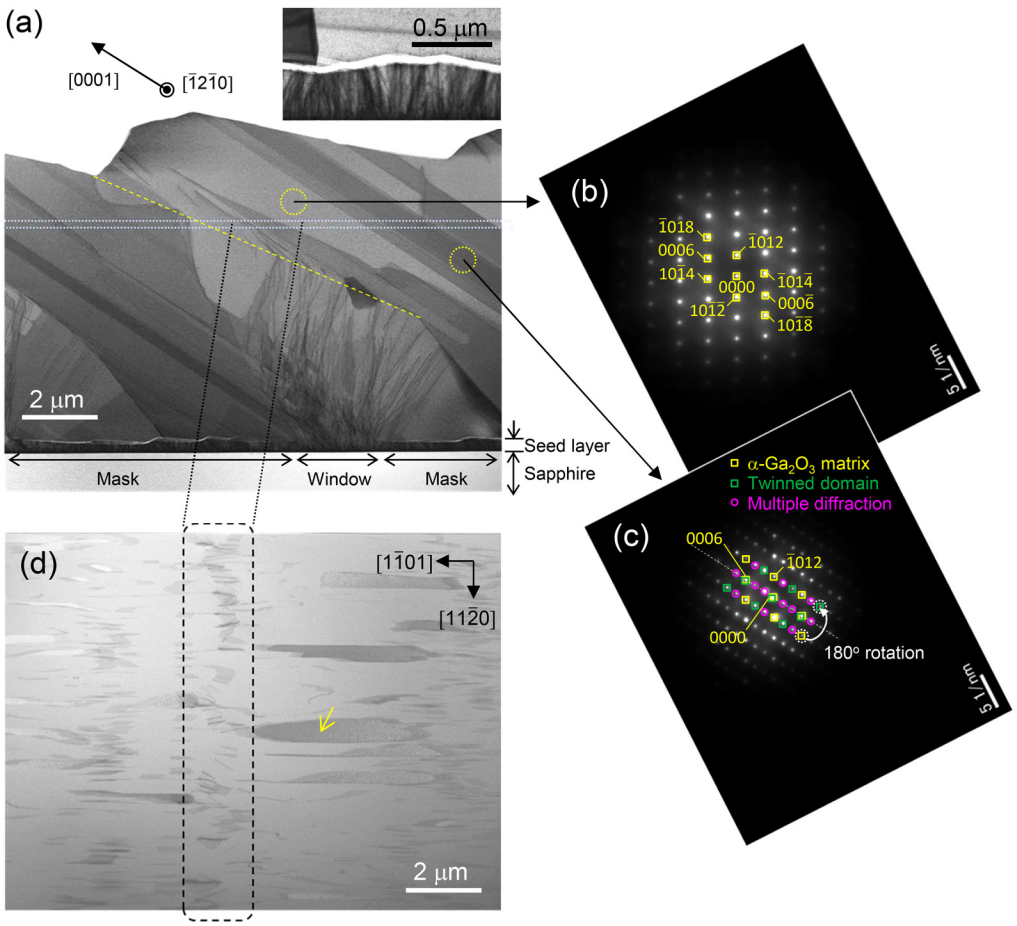

FIG. 3. (a) Cross-sectional bright-field TEM image of the coalesced α-Ga_2O_3 film grown for 2 h. The rectangle shows the depth from which the plan-view TEM specimen was cut. The inset shows a magnified image of the seed layer. (b) and (c) SAED patterns of the circled areas in panel (a). (d) Plan-view bright-field TEM image of the film.

high-quality areas, and the formation of high dislocation density areas is avoided. However, this method is costly because this process requires two rounds of photolithography and epitaxial growth, as well as a polishing process prior to the second growth.

In the present work, we report on the remarkable reduction of the high dislocation density areas by a single ELO process by performing the growth on an *r*-plane sapphire substrate with an appropriate mask design.

II. EXPERIMENTAL

α-Ga_2O_3 was grown by the conventional ELO technique on a ($\bar{1}012$) (*r*-plane) sapphire substrate with an α-Ga_2O_3 seed layer with a thickness of approximately 350 nm. We used a striped mask pattern along $\langle\bar{1}2\bar{1}0\rangle$ with mask/window widths of 5/5 μm. Conventional HVPE was used for the growth using $GaCl_x$ and O_2 as the precursors. The partial pressures of $GaCl_x$ and O_2 supply were 1.25×10^{-1} and 1.25 kPa, respectively. N_2 was used as the carrier gas. The growth was performed at 520 °C under atmospheric pressure. The details of the growth conditions have been described elsewhere.[23] The morphologies of the grown crystals were observed by field-emission scanning electron microscopy (FE-SEM) with Hitachi SU8230. Transmission electron microscopy (TEM) was used to investigate the behavior of the dislocations. The measurement was performed by JEOL JEM-2100F operated at 200 kV. The TEM samples were prepared by a focused ion beam with a thickness of approximately 200 nm. The crystal orientation was investigated by selective area electron diffraction (SAED) and x-ray pole figure measurement. The XRD measurement was performed by PANanalytical X'-pert MRD with Cu-$K_{\alpha1}$ radiation.

III. RESULTS AND DISCUSSION

Figures 1(a)–1(c) show bird's-eye view SEM images of the growth evolution. Isolated α-Ga_2O_3 stripes were formed selectively on the windows [Fig. 1(a)]. The stripes had an asymmetric

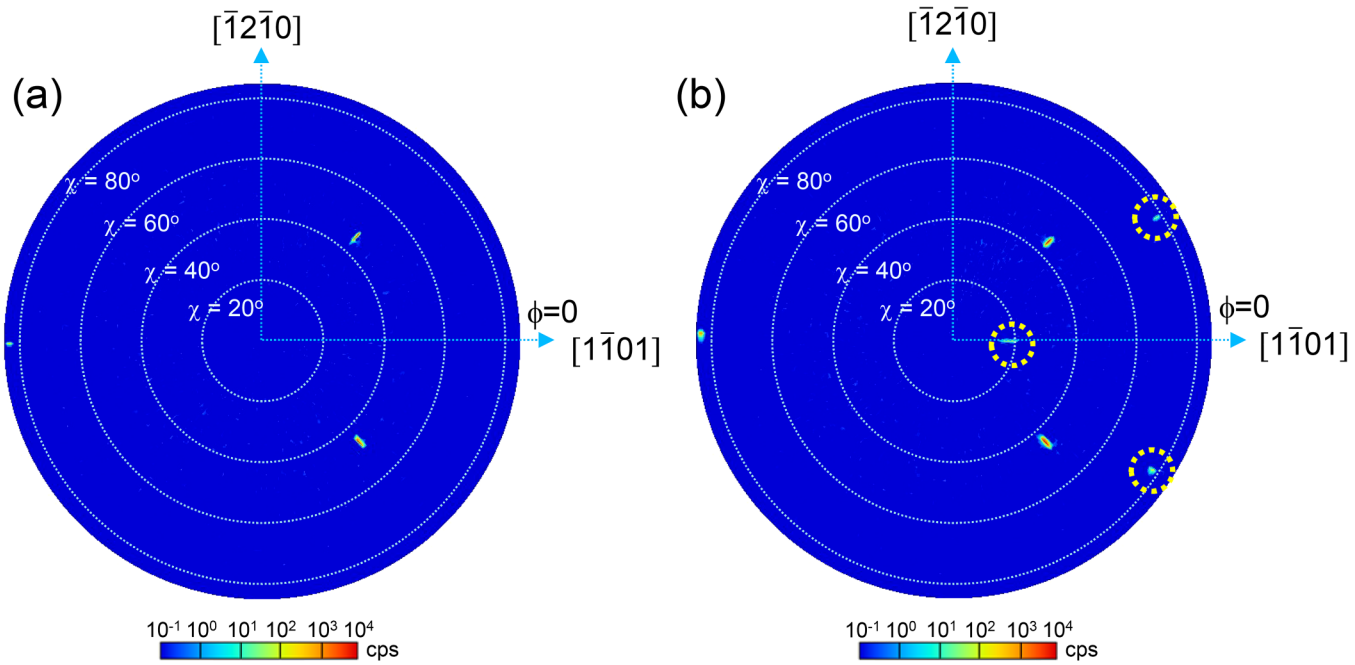

FIG. 4. X-ray pole figures (log-scale) of (a) sapphire $\bar{1}012$ and (b) α-Ga_2O_3 $\bar{1}012$.

cross-sectional shape with an inclined top surface, in contrast to conventional *c*-, *a*-, and *m*-plane α-Ga_2O_3. The stripes grew vertically and laterally to coalesce with each other [Fig. 1(b)]. Macro-scale steps and inclined terraces were formed on the coalesced surface because of the asymmetric shape. The macro-step and terrace structure was maintained throughout the growth after the coalescence, and they moved laterally like traveling waves as the growth proceeded [Fig. 1(c)]. Note that the initial acute shape of the macro-steps became smoother after the long-time growth. This morphological change took place probably to minimize the surface energy. Further long-time growth could result in a much smoother surface, which should be easily flattened by chemical mechanical polishing in contrast to the case of *c*-plane FIELO.

Figure 2(a) shows a cross-sectional SEM image of the α-Ga_2O_3 stripe grown on *r*-plane sapphire. The top surface was ($\bar{1}011$), and the side facets were ($10\bar{1}1$). On the other hand, Fig. 2(b) shows a cross-sectional SEM image of an α-Ga_2O_3 stripes along [$\bar{1}2\bar{1}0$] grown on *c*-plane sapphire. The stripes were composed of ($\bar{1}011$) and ($10\bar{1}1$) planes. Figure 2(c) schematically describes these facet structures. The *r*-plane stripes and *c*-plane stripes are drawn along the common *c* axis. This schematic tells us that the both stripes have basically the same facet structure. Note that the facet structures close to the bottom parts were different. This difference is probably because the conditions to minimize the sum of the surface energy and interface energy are different depending on the crystal orientation.

Figure 3(a) shows a cross-sectional bright-field TEM image of the coalesced film shown in Fig. 1(c). A high density of dislocations was observed in the seed layer as shown in the inset. The density was estimated to be approximately $1.4 \times 10^{10}\,cm^{-2}$. The dislocations propagated into the regrown α-Ga_2O_3 through the window as was observed for the cases of *c*-, *a*-, and *m*-plane α-Ga_2O_3. However, the dislocations bent toward the [0001] direction, and the density largely decreased at the surface. The kinks of the dislocation lines were located along the dashed line, which should be the locus of the bottom edge of the macro-step. Note that belt-like contrasts were observed along the *c* axis. SAED patterns of these parts [Figs. 3(b) and 3(c)] revealed that the dark-contrast area included twinned domains, which were rotated by 180° around the *c* axis. In Fig. 2(c), the diffraction spots from both the α-Ga_2O_3 matrix and twinned domains were observed at the same time while only diffraction spots from the α-Ga_2O_3 matrix were observed in Fig. 3(b). Figure 3(d) shows a plan-view bright-field TEM image of a specimen cut from the depth indicated by the rectangle in Fig. 3(a). Again, twinned domains were observed as the dark-contrast areas. One of the twinned domains is indicated by the arrow as an example. Dislocations were observed virtually only in the dashed frame with a liner density of approximately $7 \times 10^{4}\,cm^{-1}$, as expected from the cross-sectional observation. The areal dislocation density of the ELO-grown layer was estimated to be approximately $5 \times 10^{7}\,cm^{-2}$ from the plan-view TEM image. The identification of the dislocation character would be carried out as our future work.

Figures 4(a) and 4(b) show the x-ray pole figures of the sapphire substrate and ELO-grown α-Ga_2O_3 film, respectively. In Fig. 4(a), three diffraction spots of sapphire $\bar{1}012$ were observed at the positions that were expected for a single crystalline corundum structure. However, in Fig. 4(b), three additional weak spots (marked by dashed circles) were observed. The intensities of the

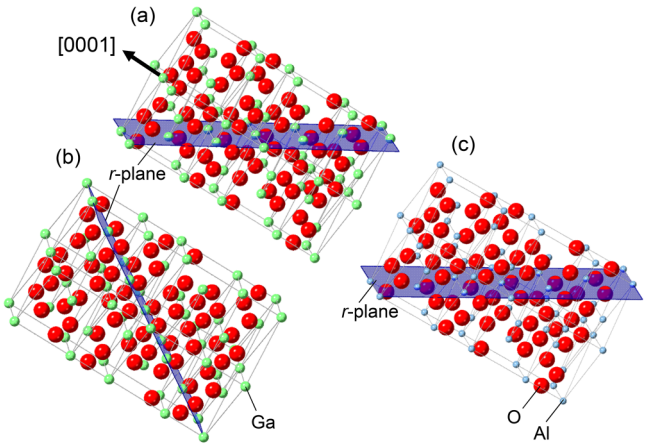

FIG. 5. Schematic of the epitaxial relationship between (a) the α-Ga_2O_3 matrix, (b) twinned α-Ga_2O_3 domains, and (c) sapphire substrate.

additional peaks were approximately an order of magnitude lower than those of the main peaks. These additional spots were explained consistently by the existence of the twinned domains around the *c* axis. This result agreed with that of the TEM investigation. Note that such twinned domains were also found in the *r*-plane α-Ga_2O_3 seed layer by x-ray pole figure measurement (not shown). Therefore, the twinned domains in the regrown layer were proposed to originate from those in the seed layer. Hence, the growth conditions of the seed layer need to be improved to suppress the twinning.

Figure 5 shows the epitaxial relationship between the α-Ga_2O_3 matrix, twinned α-Ga_2O_3 domains, and sapphire substrate determined by the SAED/pole figure measurements. The α-Ga_2O_3 matrix and sapphire substrate have the same orientation, i.e., $(0001)_{Ga2O3} \parallel (0001)_{sap}$ and $[\bar{1}2\bar{1}0]_{Ga_2O_3} \parallel [\bar{1}2\bar{1}0]_{sap}$. On the other hand, the twinned domain was rotated around the *c* axis by 180°, i.e., $(0001)_{Ga2O3} \parallel (0001)_{sap}$ and $[1\bar{2}10]_{Ga_2O_3} \parallel [\bar{1}2\bar{1}0]_{sap}$.

Figures 6(a) and 6(b) are the cross-sectional schematics showing the growth models of conventional *c*-plane ELO and *r*-plane ELO in the present work, respectively. In the case of *c*-, *a*-, and *m*-plane ELO [Fig. 6(a)], a high dislocation density area remained on the surface above the window because the dislocations in the seed layer went up straight through the window. However, in the case of the *r*-plane [Fig. 6(b)], each domain grew toward the inclined direction so as to cover the adjacent domain. In this growth process, the dislocations first propagated so that they were approximately perpendicular to the $(\bar{1}011)$ top surface to minimize the elastic energy along the dislocation lines. After that, when they met the bottom edge of the macro-step on the dashed line, they bent toward the *c* axis to follow the macro-step. As a result, the dislocations were concentrated in a narrow area along the *c* axis, and then pair annihilation should be enhanced. Although dislocations still remained on the top surface, the density was much lower than those on the windows for the case of ELO on the conventional planes.

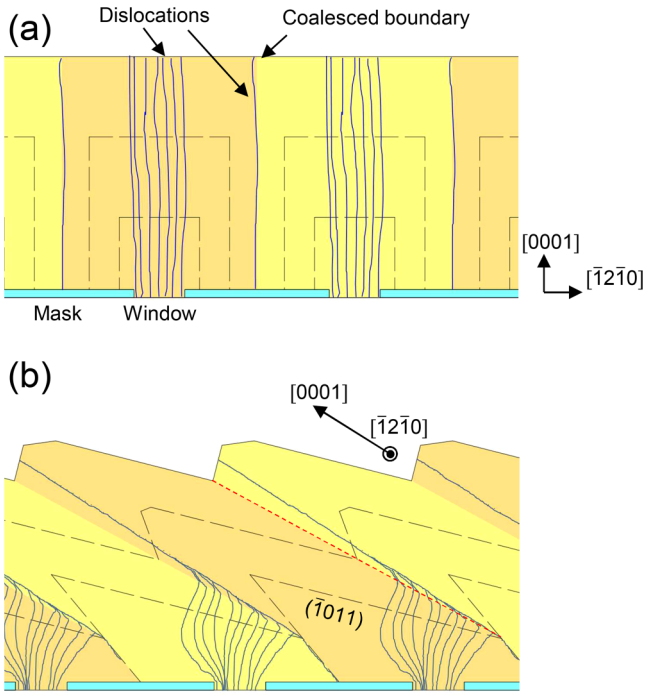

FIG. 6. Cross-sectional schematics of α-Ga_2O_3 films grown on (a) a *c*-plane substrate with a striped mask along [1$\bar{1}$00] and (b) an *r*-plane substrate with a striped mask along [1$\bar{2}\bar{1}$0].

IV. SUMMARY

We demonstrated the ELO of *r*-plane α-Ga_2O_3 using a striped mask pattern along $\langle\bar{1}2\bar{1}0\rangle$, and a coalesced compact film was successfully achieved. The α-Ga_2O_3 stripes formed at the initial growth stage exhibited an asymmetric cross-sectional stripe shape. The asymmetric shape led to a wave-like morphology of the coalesced film, and this was maintained throughout the growth. Cross-sectional TEM observation revealed that each domain grew toward the inclined [0001] direction so as to cover the adjacent domain. As a result, although the dislocations propagated into the regrown α-Ga_2O_3, they bent toward the *c* axis to concentrate in a narrow area, leading to the effective pair annihilation. Thus, this technique enabled a much-improved crystal quality at the surface in contrast to the case of conventional *c*-, *a*-, and *m*-plane ELO where dislocations go up straight to the top surface through the window to form high dislocation density areas.

ACKNOWLEDGMENTS

This work was supported by Innovative Science and Technology Initiative for Security (JPJ004596), ATLA, Japan.

AUTHOR DECLARATIONS

Conflict of Interest

The authors have no conflicts to disclose.

DATA AVAILABILITY

The data that support the findings of this study are available within the article.

REFERENCES

[1]D. Shinohara and S. Fujita, Jpn. J. Appl. Phys. **47**, 7311 (2008).
[2]M. Oda, R. Tokuda, H. Kambara, T. Tanikawa, T. Sasaki, and T. Hitora, Appl. Phys. Express **9**, 021101 (2016).
[3]T. Maeda, M. Okigwa, Y. Kato, I. Takahashi, and T. Shinohe, AIP Adv. **10**, 125119 (2020).
[4]M. Lee, M. Yang, H. Lee, H. U. Lee, H. Lee, H. Son, and U. J. Kim, Mater. Sci. Semicond. Process. **123**, 105565 (2021).
[5]J. Bae, D. Jeon, J. Park, and J. Kim, J. Vac. Sci. Technol. A **39**, 033410 (2021).
[6]S. Fujita and K. Kaneko, J. Cryst. Growth **401**, 588 (2014).
[7]R. Wakabayashi, K. Yoshimatsu, M. Hattori, J. Lee, O. Sakata, and A. Ohtomo, Cryst. Growth Des. **21**, 2844 (2021).
[8]K. Kaneko, S. Fujita, and T. Hitora, Jpn. J. Appl. Phys. **57**, 02CB18 (2018).
[9]S. Kan, S. Takemoto, K. Kaneko, I. Takahashi, M. Sugimoto, T. Shinohe, and S. Fujita, Appl. Phys. Lett. **113**, 212104 (2018).
[10]J. G. Hao, H. H. Gong, X. H. Chen, Y. Xu, F. Ren, S. L. Gu, R. Zhang, Y. D. Zheng, and J. D. Ye, Appl. Phys. Lett. **118**, 261601 (2021).
[11]K. Kaneko, Y. Masuda, S. Kan, I. Takahashi, Y. Kato, T. Shinohe, and S. Fujita, Appl. Phys. Lett. **118**, 102104 (2021).
[12]FLOSFIA and Kyoto University, News release, July 13, 2018, see http://flosfia.com/20180713/.
[13]FLOSFIA and Kyoto University, News release, July 13, 2019, see https://flosfia.com/20191202-2/.
[14]D. Machon, P. F. McMillan, B. Xu, and J. Dong, Phys. Rev. B **73**, 094125 (2006).
[15]A. Kuramata, K. Koshi, S. Watanabe, Y. Yamaoka, T. Masui, and S. Yamakoshi, Jpn. J. Appl. Phys. **55**, 1202A2 (2016).
[16]Z. Galazka, K. Irmscher, R. Uecker, R. Bertram, M. Pietsch, A. Kwasniewski, M. Naumann, T. Schulz, R. Schewski, D. Klimm, and M. Bickermann, J. Cryst. Growth **404**, 184 (2014).
[17]K. Hoshikawa, E. Ohba, T. Kobayashi, J. Yanagisawa, C. Miyagawa, and Y. Nakamura, J. Cryst. Growth **447**, 36 (2016).
[18]E. G. Víllora, K. Shimamura, Y. Yoshikawa, K. Aoki, and N. Ichinose, J. Cryst. Growth **270**, 420 (2004).
[19]Y. Oshima, E. G. Víllora, and K. Shimamura, Appl. Phys. Express **8**, 055501 (2015).
[20]A. I. Pechnikov, S. I. Stepanov, A. V. Chikiryaka, M. P. Scheglov, M. A. Odnobludov, and V. I. Nikolaev, Semiconductors **53**, 780 (2019).
[21]H. Son and D. W. Jeon, J. Alloys Compd. **773**, 631 (2019).
[22]Z. Cheng, M. Hanke, P. Vogt, O. Bierwagen, and A. Trampert, Appl. Phys. Lett. **111**, 162104 (2017).
[23]Y. Oshima, K. Kawara, T. Shinohe, T. Hitora, M. Kasu, and S. Fujita, APL Mater. **7**, 022503 (2019).
[24]K. Akaiwa, K. Kaneko, K. Ichino, and S. Fujita, Jpn. J. Appl. Phys. **55**, 1202BA (2016).
[25]H. Son, Y. Choi, J. Ha, S. Jung, and D. Jeon, Cryst. Growth Des. **19**, 5105 (2019).
[26]Y. Oshima, K. Kawara, T. Oshima, M. Okigawa, and T. Shinohe, Jpn. J. Appl. Phys. **59**, 025512 (2020).
[27]A. N. Cha, S. Bang, H. Rho, H. Bae, D. W. Jeon, J. W. Ju, S. K. Hong, and J. S. Ha, Appl. Phys. Lett. **115**, 091605 (2019).
[28]R. Jinno, N. Yoshimura, K. Kaneko, and S. Fujita, Jpn. J. Appl. Phys. **58**, 120912 (2019).
[29]G. T. Dang, T. Yasuoka, and T. Kawaharamura, Appl. Phys. Lett. **119**, 041902 (2021).
[30]A. Usui, H. Sunakawa, A. Sakai, and A. A. Yamaguchi, Jpn. J. Appl. Phys. **36**, L899 (1997).
[31]K. Kawara, Y. Oshima, M. Okigawa, and T. Shinohe, Appl. Phys. Express **13**, 075507 (2020).